Princeton Plasma Physics Laboratory

PPPL-5151

Optimization of the angular orientation for a fast ion loss detector in a tokamak

D. S. Darrow

July 2015

Prepared for the U.S. Department of Energy under Contract DE-AC02-09CH11466.

Princeton Plasma Physics Laboratory
Report Disclaimers

Full Legal Disclaimer

Trademark Disclaimer

PPPL Report Availability

Princeton Plasma Physics Laboratory:

http://www.pppl.gov/techreports.cfm

Office of Scientific and Technical Information (OSTI):

http://www.osti.gov/scitech/

Related Links:

U.S. Department of Energy

U.S. Department of Energy Office of Science

U.S. Department of Energy Office of Fusion Energy Sciences

Optimization of the angular orientation for a fast ion loss detector in a tokamak

D. S. Darrow
Princeton Plasma Physics Laboratory, Princeton, NJ 08543, USA

Abstract: A scintillator type fast ion loss detector measures the gyroradius and pitch angle distribution of superthermal ions escaping from a magnetically confined fusion plasma at a single location. Described here is a technique for optimizing the angular orientation of such a detector in an axisymmetric tokamak geometry in order to intercept losses over a useful and interesting ranges of pitch angle. The method consists of evaluating the detector acceptance as a function of the fast ion constants of motion, i.e. energy, canonical toroidal momentum, and magnetic moment. The detector acceptance can then be plotted in a plane of constant energy and compared with the relevant orbit class boundaries and fast ion source distributions. Knowledge of expected or interesting mechanisms of loss can further guide selection of the detector orientation. The example of a fast ion loss detector for the National Spherical Torus Experiment-Upgrade (NSTX-U) [J.E. Menard *et al., Nucl. Fusion* **52** 083015 (2012)] is considered.

1. Introduction

Fast ion loss detectors for magnetically confined fusion plasmas can provide valuable information on the total loss rate, and the energy and pitch angle distributions of the loss as a function of time. A particle's pitch angle is the angle between its instantaneous velocity vector and the magnetic field at the particle's position. The lost ions may be neutral beam heating ions, radiofrequency heated tail ions, or charged fusion products. Knowledge of the loss parameters is important both for the general engineering considerations of wall heating and the associated loss of plasma heating, and also for understanding the mechanisms by which the fast ions have been lost. For the latter, details of the pitch angle distribution of the loss can be particularly informative, and detectors, particularly scintillator type[1-12] are often designed to provide the best possible angular resolution and range of angular acceptance. The pitch angle resolution is a function of the entrance aperture geometry. The range of acceptance is a function both of the aperture geometry and the orientation of the apertures.

2. Method

In an axisymmetric plasma, such as a tokamak, as long as the fast ion collisionality is low, the particle guiding center orbits are completely determined, aside from position in toroidal angle, by the three constants of the motion: $E=1/2\ mv^2$, $\mu=mv_\perp^2/2B$, and $P_\phi=mRv_\phi-q\psi$, plus the sign of the particle parallel velocity relative to the plasma current. Here $v_\perp$ designates the component of the particle's velocity perpendicular to the local magnetic field, q is the ion charge and ψ is the poloidal flux at the guiding center position. For lost ions, consideration can be focused solely on co-going ions (relative to the plasma current) as these particles' orbits are shifted outward in major

radius, toward the vessel wall, where they are most likely to be lost. The formulation just described is essentially the same as the guiding center representation for particle orbits and it remains valid as long as the scale length for changes in the magnetic field strength or curvature are large compared to a fast ion gyroradius. This construction reduces the dimensionality of the fast ion phase space from six to three dimensions. In this reduced phase space, it is possible to represent important orbit class boundaries, such as the passing/trapped boundary, along with domains of loss to the inner and outer wall. Furthermore, the detector acceptance can readily be computed in this reduced space. The fast ion source function can also similarly be represented in this same space. A further reduction in dimensionality of the problem can be achieved if one examines a planar slice of the space. This allows direct plotting of the all the relevant parameters on a page or screen for easy visualization. Because an extensive past history of fast ion loss measurements in NSTX[13] has shown predominantly the loss of full energy or near full energy neutral beam ions, the typical (MHD-related) loss processes can be thought of as loosely energy-conserving. In this circumstance, a convenient and relevant choice in evaluating detector configurations is to use a plane of constant energy, the injection energy.

3. Application to NSTX-U detector

While general concepts have been discussed in the foregoing section, the specific example of the fast ion loss detector (or so-called sFLIP for "scintillator Fast Lost Ion Probe"[12] for NSTX-U[14] is elaborated upon here in some detail to demonstrate the method.

The NSTX-U project has been developed in order to improve substantially the range of plasma performance accessible in spherical tokamaks. This has been accomplished by the manufacture of a new coil system that allows double the plasma current and toroidal field strength, and installation of an additional beam line to double the neutral beam heating power of the original NSTX. The net result is to take these parameters to 2 MA, 1 T, and 15 MW, respectively. Adding the second set of neutral beams required a major modification of the large midplane port at Bay J, previously used for sFLIP, such that the diagnostic could no longer remain in its position there. A new, smaller midplane port at Bay I (displaced an additional 30 degrees toroidally further from the beam injection port) was made available for sFLIP to use on NSTX-U. This port has a purely radial center line, in the midplane. A variety of considerations led to the conclusion that re-use of the scintillator support frame, aperture assembly, and protective graphite tile on NSTX-U was the appropriate choice for reconfiguration of the diagnostic. These structures together had a total thickness of 75.6 mm. This thickness was just sufficient to satisfy an engineering requirement that the surface of the protective graphite tile lie at a major radius of at least 5 mm larger than that of the High Harmonic Fast Wave (HHFW) antenna at the midplane. The latter constraint was to insure that the antenna remained as the effective limiter in the outer midplane regardless of the detailed parameters of operation of the plasma. This requirement obliged the scintillator plate to lie in a vertical plane, and left one free parameter to be chosen, the angle of inclination of the entrance apertures relative to horizontal, i.e. the angle θ shown in Figure 1.

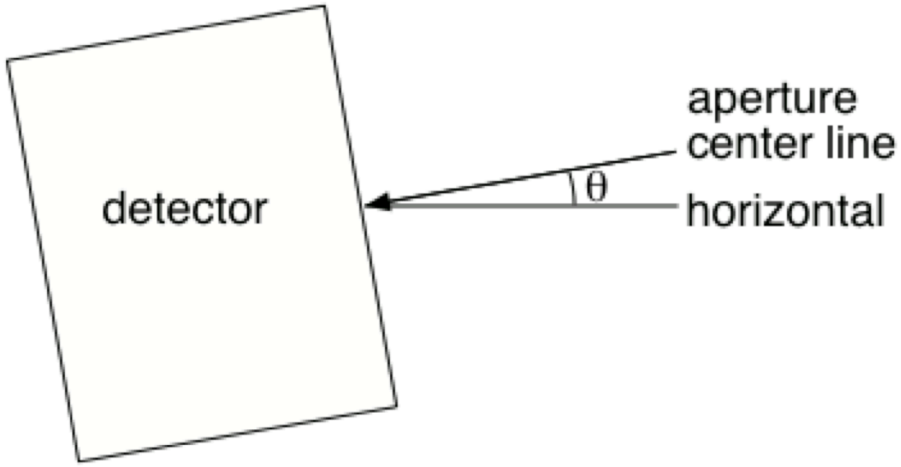

Figure 1: Diagram of the sFLIP detector on the outer midplane vessel wall, as seen from the plasma. The angle of elevation of the centerline of the apertures above horizontal, designated as θ in the figure, is the angle to be optimized. Beam ions enter in the direction shown by the arrow.

To apply the technique to optimization of θ for NSTX-U, first a single historical magnetic equilibrium is considered, and θ is varied. As a starting point, consider a past equilibrium from NSTX shot 141719 at 390 ms. This plasma had I_p=0.9 MA and B_{T0}=0.54 T, typical of NSTX plasmas and in a range where NSTX-U is likely to make its initial plasmas before advancing to higher plasma current and toroidal field.

Figure 2 shows the 90 keV slice of D beam ion phase space, plotted against P_ϕ and μ. 90 keV is the standard operating energy for the neutral beams on NSTX and NSTX-U. Depicted in this figure are the passing/trapped orbit boundary, the guiding center orbits reaching the wall at the inner and outer midplane, the set of FLR orbits reaching the wall at the outer midplane, the locus of guiding centers passing through the magnetic axis, and the set of orbits reaching the detector when θ=0°. These boundaries are computed according to formulae detailed in Refs. 15 and 16. Trapped (banana) orbits lie in the area between the passing/trapped boundary curve and the curve designating orbits lost to the outer wall. Discrete points along the sFLIP aperture acceptance curve indicate where various pitch angle particles would appear. The total angular acceptance range of the sFLIP apertures is 72°. The physical structure of the probe is likely to block orbits whose pitch angles are lower than ~15°. Hence, the aim of this design optimization effort is to orient the probe such that its 72° of useful acceptance will map to a physically interesting range of pitch angles over the variety of plasma conditions anticipated in NSTX-U.

The interesting ranges of pitch angle are determined by two factors: the beam deposition location in this phase space, and the patterns of transport of the beam ions by various phenomena. With regard to the former, beam deposition modeling for NSTX plasmas has shown that the co-injected beam ions tend to be born in the neighborhood of the right half of the "guiding centers passing through magnetic axis" parabola, typically with values of the normalized magnetic moment ranging from 0 to 1.2.[17] This range of deposition will be somewhat broadened with the addition of three new neutral beam sources introduced for NSTX-U experiments. These latter will inject at tangency radii of 1.1, 1.2, and 1.3 m, compared to a typical magnetic axis radius of 1.0 m and the tangency radii of the existing neutral beam sources of 0.5, 0.6, and 0.7 m.

The phenomena that transport beam ions are predominantly MHD instabilities. These typically are non-axisymmetric perturbations of the magnetic field in the plasma. Though these perturbations can be small ($\leq 10^{-3}$ of the confining fields), they can degrade or destroy conservation of the canonical toroidal momentum, P_ϕ. This can allow particles to be transported along horizontal lines in the space depicted in Fig. 2. and, especially, to be transported from the region where the beam ions are ionized to the detector or the vessel wall. This concept, in its simplest form, namely imagining that this horizontal transport occurs by infinitesimally small diffusive steps, leads to the erroneous conclusion that beam ions born in the plasma interior an transported to the left in this figure will always be lost to the vessel wall before encountering the detector. In fact, lost beam ions have been detected during MHD activity over a wide range of plasma parameters. This happens because the wall in NSTX is not axisymmetric. It may well also indicate that MHD can cause substantial radial steps within a few or even a single pass through the instability's fields, consistent with results reported by others.[18,19]

The instabilities can also alter the energy (and hence gyroradius) of the beam ions. In the case where the wavelength of the MHD perturbations are of the order or smaller than the beam ion gyroradius (~20 cm in NSTX and half that for NSTX-U), then the magnetic moment of the particles will not longer be conserved, and transport in the vertical direction in Fig. 2 can also occur. It should also be noted that points in the (P_ϕ, μ) plane above the upper leg of the passing/trapped boundary curve are physically unrealizable, so the calculated detector acceptance curves should never reach that region, nor be expected to.

Figure 2 shows that the detector acceptance at θ=0° extends from μ=0 to 1.2, but does not reach all the way to the upper limb of the passing/trapped boundary curve. Since it was desired to maximize the range of pitch angles detectable by the probe, other values of θ were also considered. Figure 3 shows the corresponding plot for θ=20°. In this case, the detector acceptance extends from μ=0.1 to 1.3, and an 80° pitch angle point appears on the detector curve. However, this arrangement appears less suitable than that with θ=0° because there is a range of low pitch angle particles which will not be recorded by the detector. In addition, it appears questionable whether the

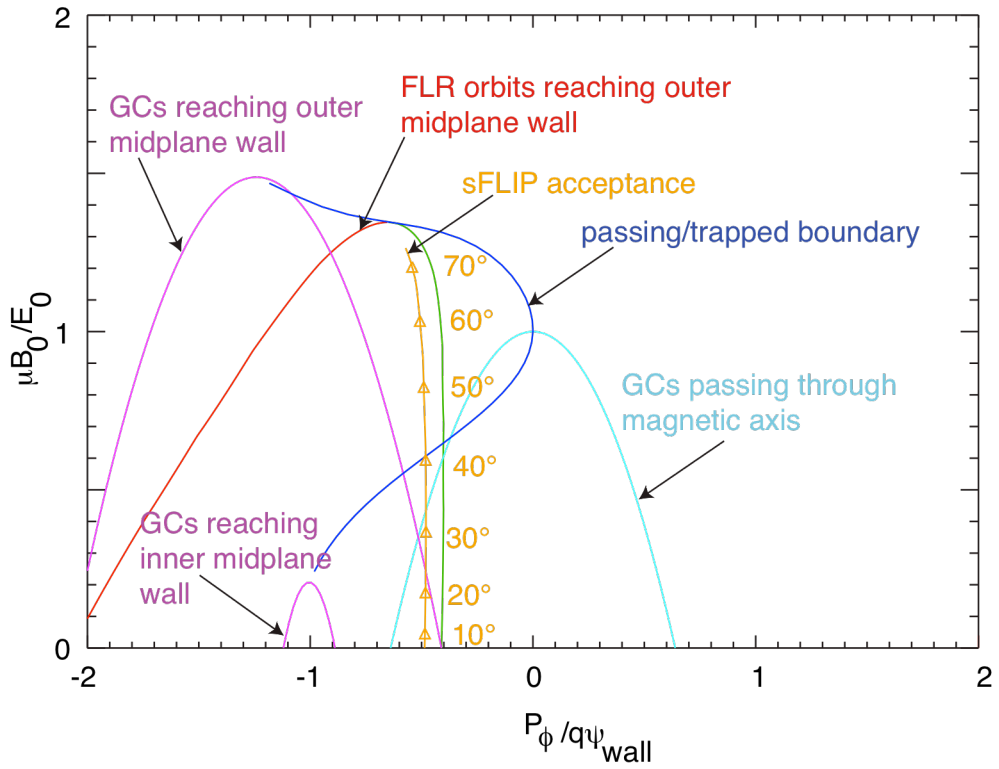

Figure 2: A slice through the D neutral beam ion phase space for the magnetic equilibrium of NSTX shot 141719 at 493 ms, for 90 keV ions. In this case, the aperture inclination angle is θ=0°. On the horizontal axis is the normalized canonical toroidal momentum, and on the vertical axis is the normalized magnetic moment, $\mu B_0/E$. Features in this phase space are as follows. The dark blue curve is the passing/trapped boundary. The tall magenta parabola is the locus of guiding centers reaching the outer midplane wall. The short magenta parabola is the locus of guiding centers reaching the inner midplane wall. The green and red curves, taken together, are the locus of guiding centers where the particle orbit (including gyromotion) reaches the outer wall (i.e. it is the finite Larmor radius corrected version of the large magenta parabola). The green half of this curve comprises co-going orbits while the red half is counter-going. The cyan parabola is the set of guiding centers that pass through the magnetic axis. Finally, the orange curve depicts the sampling volume of the sFLIP diagnostic at the selected angular orientation. The triangles along this curve denote steps of 10° in pitch angle.

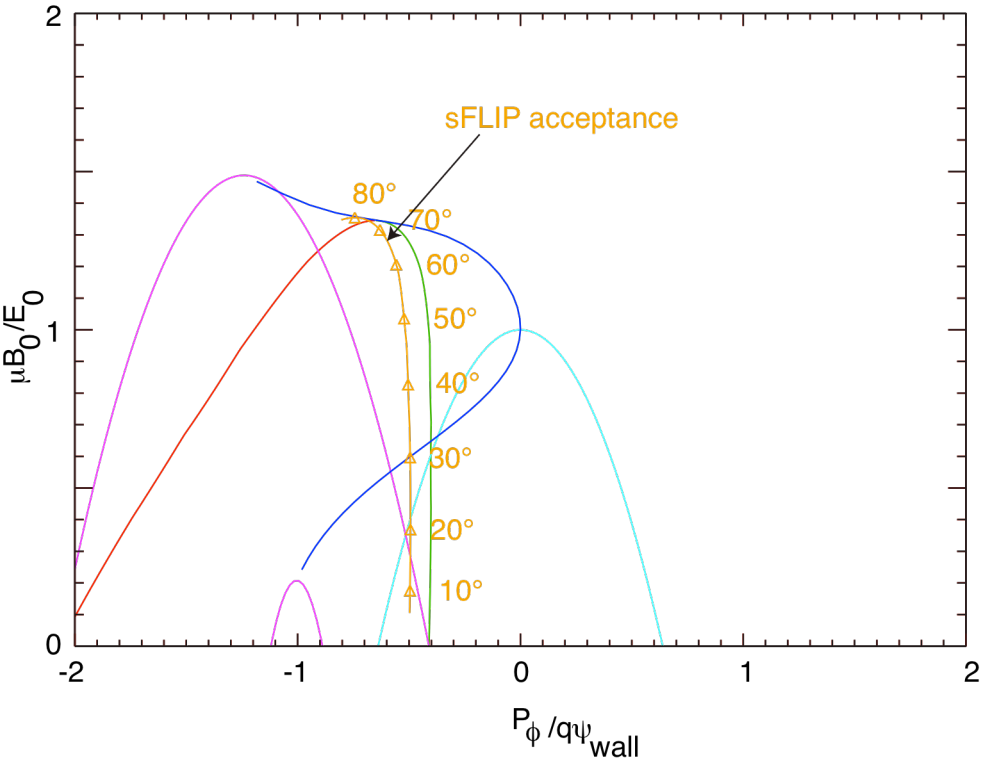

Figure 3: 90 keV slice through the D neutral beam ion phase space for the same parameters as in Fig. 2, except that the detector inclination angle is changed to θ=20°.

range of pitch angles >70° will be well enough separated on the scintillator plate to be able to distinguish them.

The question of whether negative values of θ are potentially useful is explored in Figure 4, where the curves for θ=-20° are plotted. It is clear immediately that this choice greatly diminishes the range of pitch angles registered by the detector, making this choice unsuitable. Finally, Fig. 5 shows the detector curve for θ=10°. This is the most suitable choice of θ, at least within the accuracy of the 10° steps taking here, as it accepts beam ions from very low pitch angles up to the uppermost accessible value, ~80°.

Thus far in this work, optimization of the detector orientation has proceeded using a plasma equilibrium that is typical of historical NSTX discharges. Although plasma equilibria in NSTX-U will nominally be scaled versions of those generated in NSTX, (and hence the pitch angle coverage of the detector should remain unchanged) it is worth mapping the detector acceptance for some modeled equilibria from NSTX-U to check the suitability of the chosen orientation for the projected new plasma conditions. This is done in Figures 6 through 8. As can be seen in these figures, the curve defining the acceptance range of the diagnostic also nicely spans the range from fully parallel-going particles to very perpendicular ones for all the NSTX-U conditions examined. Consequently, the detector has been mounted with θ=10° for NSTX-U.

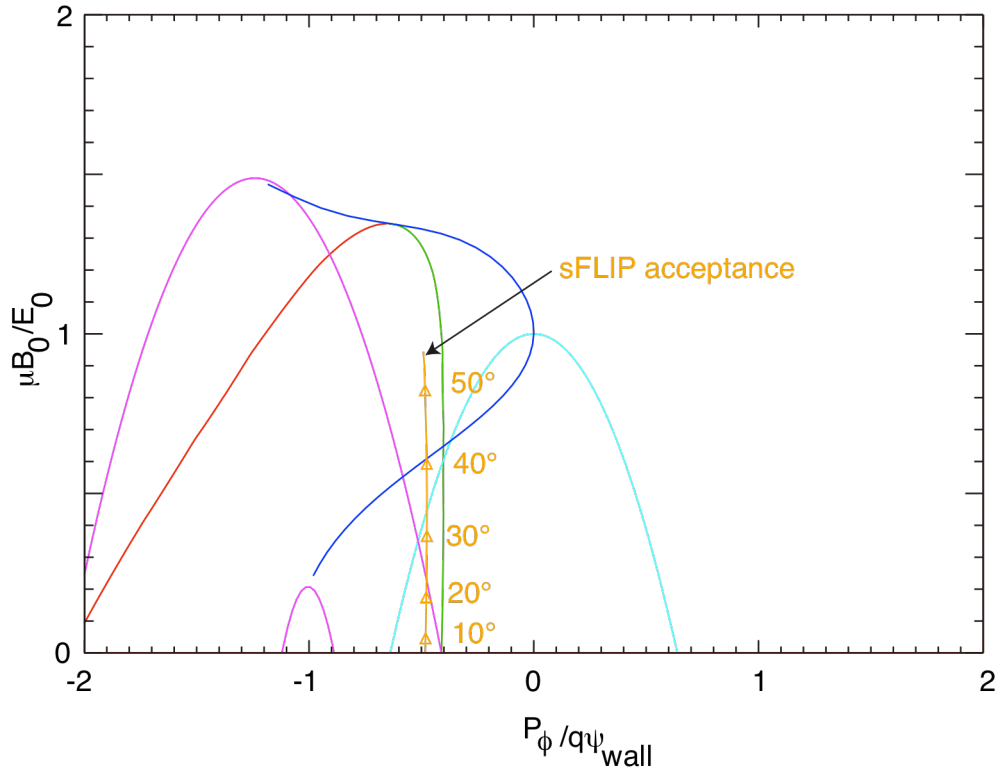

Figure 4: 90 keV slice through the D neutral beam ion phase space for the same parameters as in Fig. 2, except that the detector inclination angle is changed to θ=-20°.

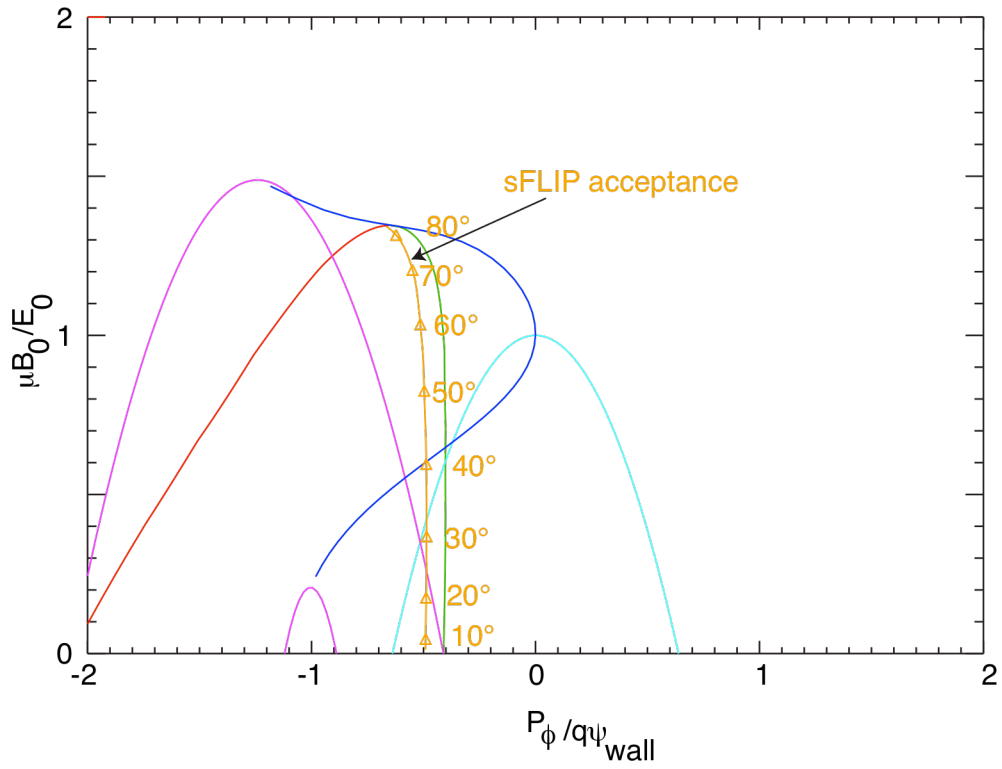

Figure 5: 90 ke V slice through the D neutral beam ion phase space for the same parameters as in Fig. 2, except that the detector inclination angle is changed to θ=10°.

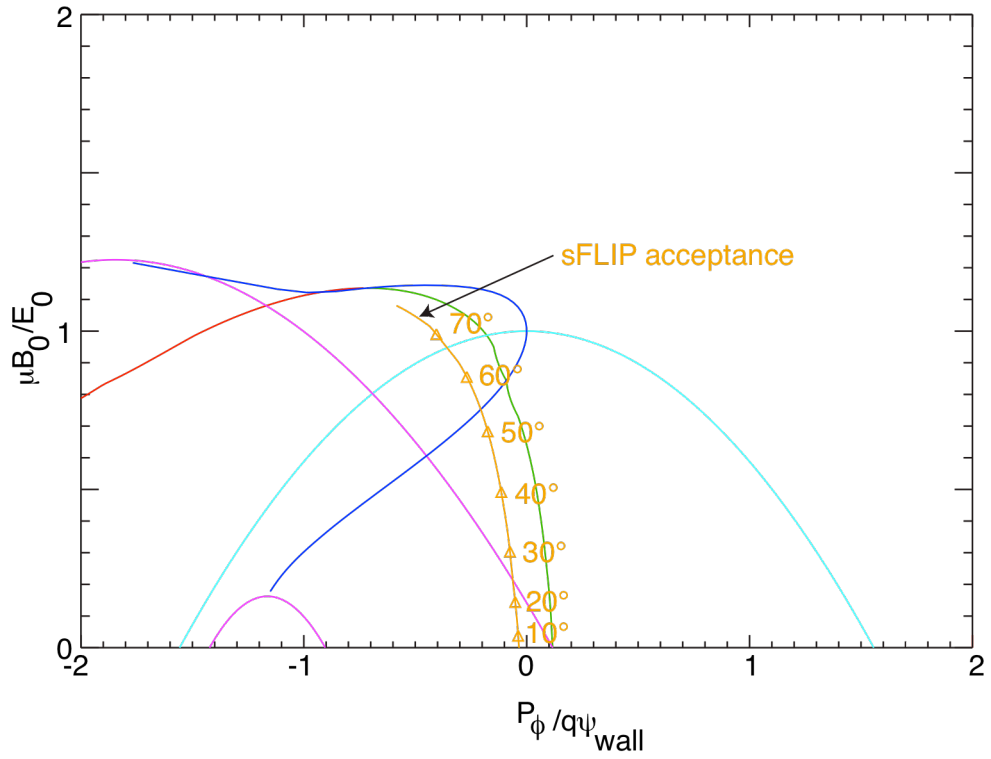

Figure 6: 90 keV slice through the D neutral beam ion phase space using an NSTX-U model equilibrium with I_p=0.8 MA and B_T=0.55 T with q=10°.

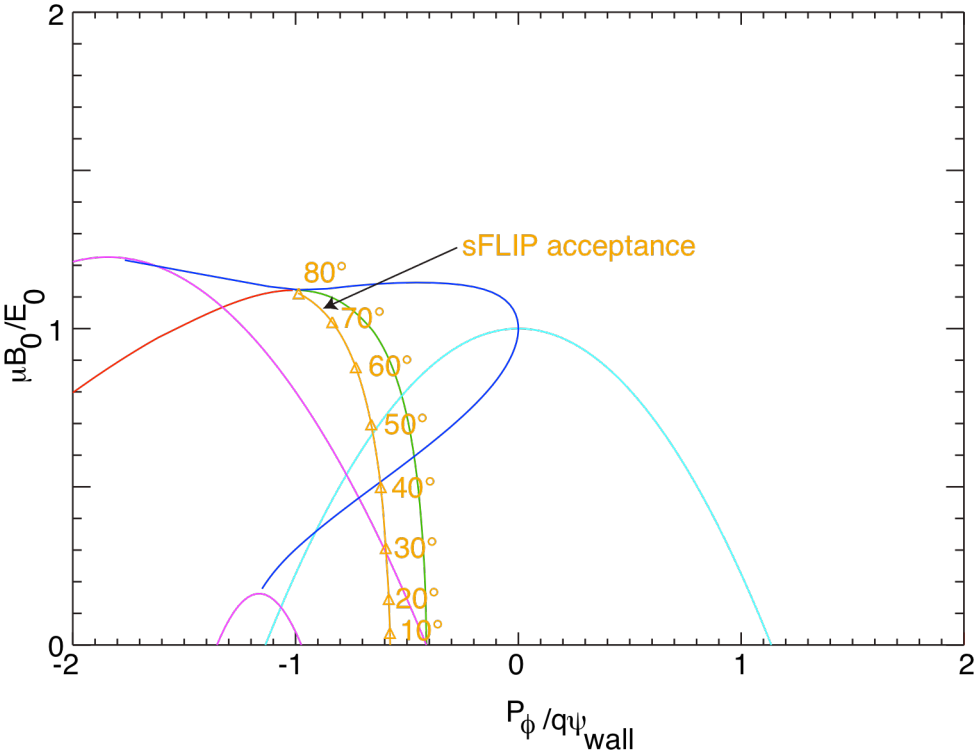

Figure 7: 90 keV slice through the D neutral beam ion phase space using an NSTX-U model equilibrium with I_p=1.5 MA and B_T=0.75 T with θ=10°.

Here, the method of considering a reduced-dimension phase space has been applied to

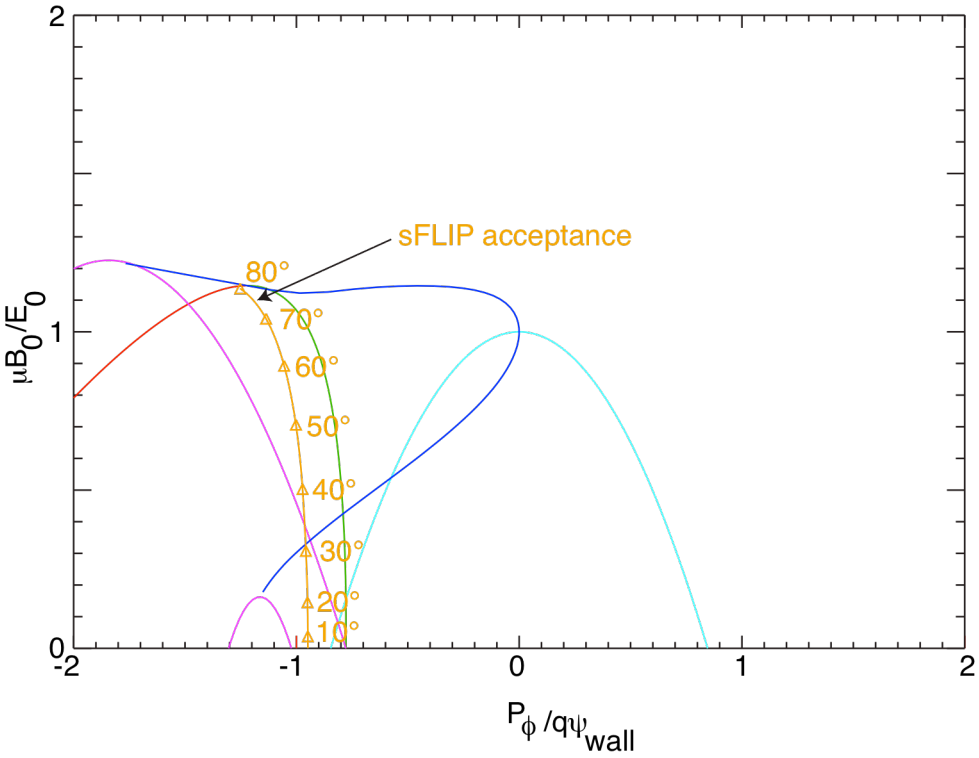

Figure 8: 90 keV slice through the D neutral beam ion phase space using an NSTX-U model equilibrium with I_p=2.0 MA and B_T=1.0 T with θ=10°.

optimization of the orientation of a scintillator type fast ion loss detector. More generally, though, the method should be applicable to virtually any type of fast ion diagnostic. In the case of other diagnostics, other optimization criteria will apply, and it would be necessary to consider details of how the diagnostic signal arises and is distributed in phase space in order to arrive at an optimization algorithm.

Acknowledgements

This work supported by US DoE Contract DE-AC0209CH11466.

References

[1]S. J. Zweben, R. L. Boivin, M. Diesso, *et al*., *Nucl. Fusion* **30**, 1551 (1990).
[2]D. S. Darrow, H. W. Herrmann, D. W. Johnson, R. J. Marsala, R. W. Palladino, and S. J. Zweben, *Rev. Sci. Instrum.* **66**, 476 (1995).
[3]D. S. Darrow, M. Isobe, T. Kondo, M. Sasao, K. Toi, M. Osakabe, K. Matsuoka, S. Okamura, S. Kubo, C. Takahashi, and the CHS Group, *Proceedings of the Joint Conference of the 11th International Stellarator Conference and 8th International Toki Conference on Plasma Physics and Controlled Nuclear Fusion, 1997* (Japan Society of Plasma Science and Nuclear Fusion Research, Nagoya, Japan, 1998), Vol. 1, p. 362.
[4] D. S. Darrow, M. Isobe, T. Kondo, M. Sasao, CHS Group, *Rev. Sci. Instrum.* **70**, 838 (1999).

[5]D. S. Darrow, A. Werner, A. Weller, *Rev. Sci. Instrum.* **72**, 2936 (2001).
[6]M. Nishiura, M. Isobe, T. Saida, M. Sasao, D. S. Darrow, *Rev. Sci. Instrum.* **75**, 3646 (2004).
[7]K. Shinohara, H. Kawashima, K. Tsuzuki, *et al.*, *Nucl. Fusion* **43**, 586 (2003).
[8]S. Baeumel, A. Werner, R. Semler, *et al.*, *Rev. Sci. Instrum.* **75**, 3565 (2004).
[9]M. García-Muñoz, H.-U. Fahrbach, H. Zohm, and the ASDEX Upgrade Team, *Rev. Sci. Instrum.* **80**, 053503 (2009).
[10]R. K. Fisher, D. C. Pace, M. Garcia-Munoz, W. W. Heidbrink, C. M. Muscatello, M. A. Van Zeeland, and Y. B. Zhu, *Rev. Sci. Instrum.* **81**, 10D307 (2010).
Y. P. Zhang, Yi Liu, X. B. Luo, M. Isobe, G. L. Yuan, Y. Q. Liu, Y. Hua, X. Y. Song, J.
[11]W. Yang, X. Li, W. Chen, Y. Li, L. W. Yan, X. M. Song, Q. W. Yang, and X. R. Duan, *Rev. Sci. Instrum.* **85,** 053502 (2014).
[12]D. S. Darrow, *Rev. Sci. Instrum.* **79**, 023502 (2008).
[13]E.J. Synakowski, M.G. Bell, R.E. Bell, *et al., Nucl. Fusion* **43**, 1653 (2000).
[14]J. E. Menard, *et al., Nucl. Fusion* **52,** 083015 (2012)
[15]J. A. Rome and Y.-K. M. Peng, *Nucl. Fusion* **19**, 1193 (1979).
[16]C. T. Hsu and D. J. Sigmar, *Phys. Fluids B* **4**, 1492 (1992).
[17]D. S. Darrow, N. Crocker, N. N. Gorelenkov, S. Kubota, M. Podestà, L. Shi, R. White, *Plasma and Fusion Res.* **8**, 2402119 (2013).
[18]X. Chen, M. E. Austin, R. K. Fisher, W. W. Heidbrink, G. J. Kramer, R. Nazikian, D. C. Pace, C. C. Petty, and M. A. Van Zeeland, *Phys. Rev. Lett.* **110**, 069302 (2013).
[19]X. Chen, W. W. Heidbrink, G. J. Kramer, M. A. Van Zeeland, M. E. Austin, R. K. Fisher, R. Nazikian, D. C. Pace, and C. C. Petty, *Nucl. Fusion* **53**, 123019 (2013).

PPPL PRINCETON PLASMA PHYSICS LABORATORY

Princeton Plasma Physics Laboratory
Office of Reports and Publications

Managed by
Princeton University

under contract with the
U.S. Department of Energy
(DE-AC02-09CH11466)

P.O. Box 451, Princeton, NJ 08543
Phone: 609-243-2245
Fax: 609-243-2751

E-mail: publications@pppl.gov

Website: http://www.pppl.gov